FOREX Publication
Open Access | Rapid and quality publishing

International Journal of
Electrical and Electronics Research (IJEER)
Research Article | Volume 13, Issue 2 | Pages 346-352 | e-ISSN: 2347-470X

Analysis of Constant Losses of Three-Phase Squirrel Cage Induction Motor with Different Types of Eccentricity Under No Load Operating Condition

Payal Suthar[1*] and Dr. Ketan Badgujar[2]

[1]Research scholar, Gujarat Technological University, Ahmedabad, India; suthar6482_payal@yahoo.co.in
[2]Professor, Electrical Engineering Department, Gujarat Technological University, L. D. College of Engineering, Ahmedabad, India; dr.ketanbadgujar@gmail.com

***Correspondence:** *suthar6482_payal@yahoo.co.in*

ABSTRACT- This research investigates the core loss of a 5 HP three-phase squirrel cage induction motor across different levels of three types of eccentricities (static, dynamic, and mixed) utilizing Ansys Maxwell software. The simulation outcomes for core losses are compared with analytical core loss values. No load and loss separation tests conducted under healthy conditions and at 12% static, 12% dynamic, and 12% mixed eccentricities to determine constant loss and isolate the core loss from constant loss. Furthermore, the simulation and analytical findings are compared with experimental results, particularly at a rotor eccentricity of 12%.

Keywords: Core loss, Hysteresis losses, Eddy current losses, Eccentricity.

ARTICLE INFORMATION
Author(s): Payal Suthar and Dr. Ketan Badgujar;
Received: 14/04/2024; **Accepted**: 07/06/2024; **Published**: 30/06/2025;
e-ISSN: 2347-470X;
Paper Id: IJEER 1404-11;
Citation: 10.37391/ijeer.130219
Webpage-link:
https://ijeer.forexjournal.co.in/archive/volume-13/ijeer-139219.html

Publisher's Note: FOREX Publication stays neutral with regard to Jurisdictional claims in Published maps and institutional affiliations.

1. INTRODUCTION

Eccentricity in induction motors causes serious challenges for condition monitoring and diagnostics. The variation in air gap length between the stator and rotor due to the separation of their geometrical axes in a rotating machine is called eccentricity. The types of eccentricity depend on the rotation axis along which rotor rotates. In static eccentricity, the rotor rotates with its axis and the minimum air gap length is fixed with the rotor position while in case of dynamic eccentricity, the minimum air gap position changes with the rotor position as the rotor rotates with stator axis and finally mixed eccentricity consists both the effects simultaneously[1].The air gap flux density waveform is composed of numerous harmonics stemming from construction and operational factors, such as phase belt harmonics, MMF harmonics, permeance harmonics, and saturation harmonics. Even under healthy conditions with a pure sine wave supply, these harmonics are present. Additionally, eccentricity introduces additional harmonics to the stator current spectrum due to the asymmetry in air gap length. Static eccentricity generates twin harmonics near principal slot harmonics, while dynamic eccentricity introduces a frequency band around primary slot harmonics with a frequency given by *eq. (1)* as per [2].

$$f_h = \left[(R \pm n_d) \frac{(1-s)}{p} \pm \lambda \right] f_s \quad (1)$$

Where,
n_d=*0 (for static),*
n_d *= 1; 2; 3; (for dynamic),*
fs = fundamental frequency,
R = no. of rotor slots,
s =slip,
p = no. of pole pair,
λ *= 1,3,5...*

It is evident that as the degree of eccentricities increases, the amplitude of generated harmonic frequencies increases. Due to eccentricity, an air gap decreases on one side, increases the flux concentration in the core and teeth of that region, ultimately increases the iron loss and friction losses due to additional loading on the bearing[2]. The presence of eccentricity disturbs the temperature distribution through the stator and rotor core. Unbalanced radial forces are also exerted on the stator and rotor, which raise the bearing load and increase the friction losses[3].

Several methods have been proposed to find core loss, considering different criteria. Several existing models to determine core loss with different frequency and flux density range presented in [4][5]. Similarly, an overview of the Steinmetz equation, loss separation, and mathematic hysteresis loss-based loss model with its advantages and disadvantages given by [6][7] and hysteresis loss using an extended Steinmetz equation using a non-sinusoidal flux waveform explained in [8], while[9]used a loss separation algorithm to determine core loss under a non-sinusoidal supply. Investigation of iron loss of

FOREX Publication
Open Access | Rapid and quality publishing
International Journal of Electrical and Electronics Research (IJEER)
Research Article | Volume 13, Issue 2 | Pages 346-352 | e-ISSN: 2347-470X

lamination with consideration of non-sinusoidal flux density with and without minor hysteresis loop using loss separation model is explained by[10]. The analysis of core loss of different steel lamination by considering eddy current coefficient and excess loss coefficient as a function of flux density while hysteresis coefficient as a function of flux density and frequency[11].

The literature offers insights into a range of techniques for studying core losses at different frequencies and maximum flux densities. These analysis methods consider various constraints and validate their results through experimentation. The authors also discussed the impact of frequency and maximum flux density on core loss coefficients, along with presenting multiple analytical methods for calculating these coefficients. However, as far as the authors are aware, there has been no attempt to explore the effects of different types and degrees of eccentricity on constant loss components, such as core loss and mechanical loss.

This study explores the impact of eccentricity (static, dynamic, and mixed) on the no-load losses of a three-phase squirrel cage induction motor. Various degrees of static, dynamic, and mixed eccentricity are examined to analyze the changes in losses with different eccentricities. The first section of the paper calculates the no-load losses analytically for the considered degrees and types of eccentricity using time-dependent flux density[12]. The analytical model has not included the skin effect in computation of core loss because at no load current, the skin effect is less pronounced. The second section presents simulation results of the no-load losses of the induction motor with both healthy and eccentric rotors using Ansys Maxwell. The third section details the practical measurement of no-load losses at 12% static and dynamic eccentricity, as well as 12% mixed eccentricity. Finally, the fourth section of the paper discusses the comparison between analytical and simulation results of the no-load losses with practical results.

2. CORE LOSSES ANALYSIS

2.1 Analytical Determination of core losses

The basic two terms Steinmetz core loss model is given by the equation;

$$p_c = k_h f^n B^n + k_e f^2 B^2 \quad (2)$$

k_h ,k_e are hysteresis and eddy current loss coefficients, f is the frequency and B is the flux density and n is the Steinmetz constant. The Steinmetz constant considered as a 1st, 2nd, and 3rd order polynomials to modified *eq. (2)*. But Steinmetz and modified steinmetz are not suitable for flux density more than 1 T and for high frequency. Further modification has been done in core loss model by adding excess loss term, this model not used for frequency greater than 400 Hz. Hence two core loss models VARCO and CAL2 has been explored which are applicable for wide range of frequency up to 2 kHz and up to 1.5 T flux density. The simple algorithm (core loss model M) has explained with frequency range up to 4 kHz and flux density up to 1.5 T. The various models of core loss has discussed with the limitation in[4]. Core loss prediction utilizing the core loss model for sinusoidal flux density waveform gives inaccurate results because the machine exposes core lamination to non-sinusoidal flux density waveform due to their geometry and operating conditions. There are mainly two methods that are used to predict core loss for non-sinusoidal wave forms, namely frequency domain and time domain. In the frequency domain method, the FFT of the flux density wave gives the magnitude and frequency of the harmonics. The components of core loss are computed for the considered harmonic frequency. All significant harmonic losses are sum up to assess its collective impact to the core loss by using *eq. (4)*. In the time domain method, loss coefficients have been found for sinusoidal wave form because the data available from the manufacturer is for sinusoidal excitation. Utilizing these coefficients and time dependent flux density wave, core loss is computed through the application of *eq. (3)*. In this paper, analytical results of losses have been obtained by considering analytical flux density wave form through the core and teeth. The core loss equation using the time-dependent flux density approach is given by

$$P_c = p_h(B_p, f) + \mathrm{K_e}\frac{1}{T}\int_0^T \left(\frac{dB}{dt}\right)^2 dt + \mathrm{K_a}\frac{1}{T}\int_0^T \left|\frac{dB}{dt}\right|^{1.5} dt \quad (3)$$

Where; $\mathrm{K_e} = \frac{k_e}{(\sqrt{2\pi})^2}$ and $\mathrm{K_a} = \frac{k_a}{(\sqrt{2\pi})^{1.5}}$

k_e, k_a eddy current and excess loss coefficient at the peak value of flux density for the sinusoidal excitation. The core loss coefficients determined through the application of curve fitting techniques, as elaborated in[13]. The total loss equation is

$$P_c = k_h f^n B^n + k_e f^2 B^2 + k_a f^{1.5} B^{1.5} \quad (4)$$

In the next step divide the *eq. (4)* by frequency,

$$\frac{P_c}{f} = \mathrm{P} + \mathrm{Q}(\sqrt{F})^2 + \mathrm{R}(\sqrt{F}) \quad (5)$$

Where;

$\mathrm{P} = k_h B^n$
$\mathrm{Q} = k_e B^{2n}$
$\mathrm{R} = k_a B^{1.5}$

To find out the coefficients of *eq. (5)* plot the data of loss at various frequencies at specific peak flux densities for the used core material provided by the manufacturer. Practical motor used M600-50A electrical steel as per IEC60404-8-4. In this analytical calculation, the coefficients P, Q, and R have been found using the curve fitting tool of MATLAB. Then, find $\mathrm{K_h}$, $\mathrm{K_e}$, and $\mathrm{K_a}$ using P, Q, and R and calculate the losses using the value of loss coefficients in *eq. (3)*.

This study initially determines the air gap flux density waveform for all levels and types of eccentricity, followed by the determination of the core and teeth flux density waveform using the air gap flux density waveform. The analytical analysis for finding flux density wave forms the in different parts of the

FOREX Publication
Open Access | Rapid and quality publishing
International Journal of Electrical and Electronics Research (IJEER)
Research Article | Volume 13, Issue 2 | Pages 346-352 | e-ISSN: 2347-470X

motor flux density is based on the design calculation of an induction motor. The analytical and simulation results of the flux density wave forms at 12% dynamic eccentricity are illustrated in *figure 3*.

2.2 Core Loss by Ansys Maxwell

Ansys Maxwell can compute various losses in single-phase and three-phase machines. For core loss calculation, first, choose the material from the library, then set the attributes of the material. The practical motor uses M600-50A electrical steel as per IEC60404-8-4, which is not listed in the library, so it needs to be added. To add the selected material, specify its magnetic properties. The required properties are included permeability, coercivity, remanence, and saturation magnetization. You can input these values manually or select from predefined material models if available.

Figure.1 shows the parameter settings to calculate the core loss by numerical method and B-H curve of core material provided by manufacturer. *Table 1* compares the value of the loss coefficients found by analytical and Ansys Maxwell.

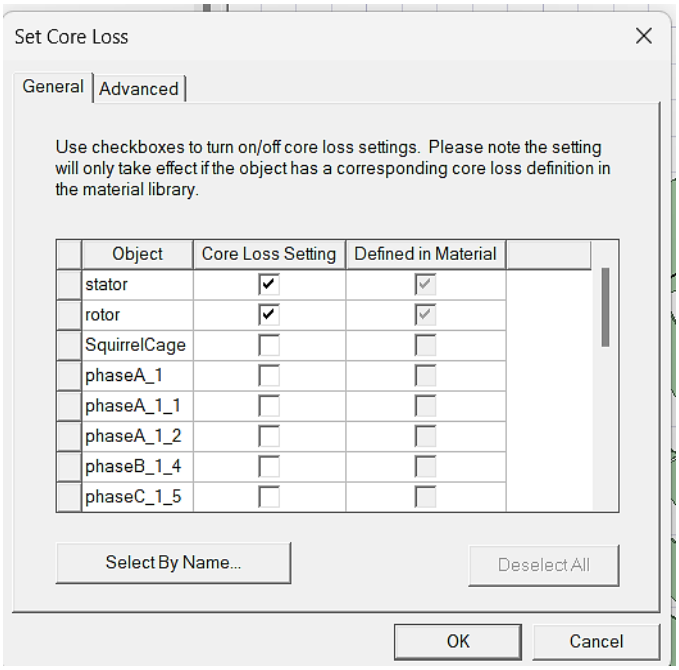

(a)

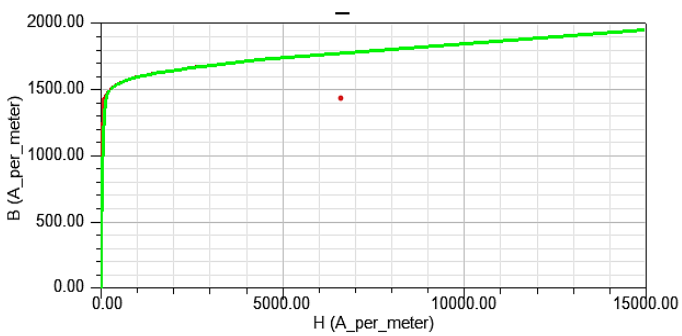

Figure 1. (a) Parameter Settings for core losses & (b) B-H curve for M45 core material

Table 1. Comparison of Analytical and Simulation value of Loss coefficients

Loss Coefficients	Analytical Results	Maxwell Results
Hysteresis loss coefficient	0.028137	0.0266
Eddy Current Loss Coefficient	$1.7871*10^{-4}$	$1.61804*10^{-4}$
Excess Loss Coefficient	$1.31643*10^{-4}$	$1.5046*10^{-4}$

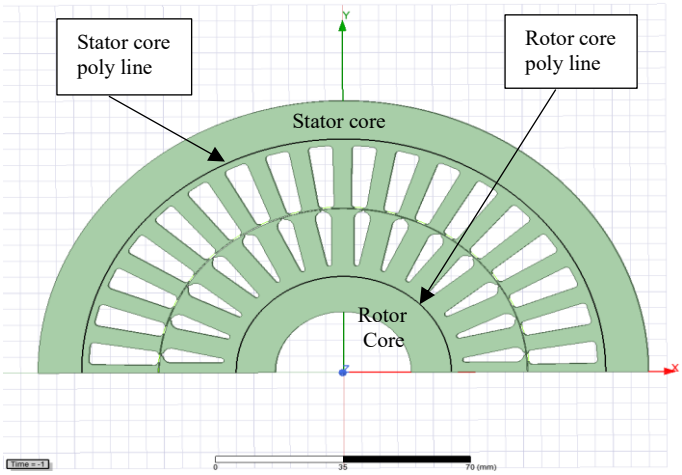

Figure 2. Polyline through stator and rolor cores

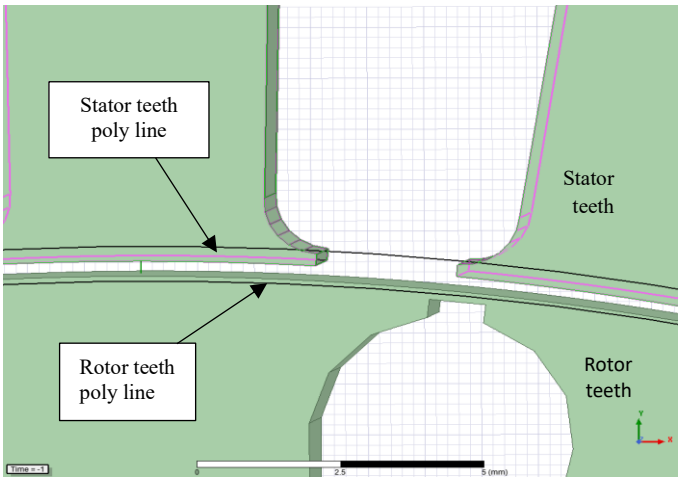

Figure 3. Polyline through stator and rolor teeth

At 12% eccentricity, the value of the average flux density is very close to the maximum value of core flux density as per B-H curve *figure 1*, so after 12% eccentricity, the change in the average value of point flux density is minimal. In order to study how the degree of eccentricity affects flux density, a specific point is established in the air gap in the direction of eccentricity. *Table 2* displays the average flux density at this point in the air gap at 10%, 12% and 13% eccentricity respectively. At an eccentricity of 12%, the average flux density closely approaches the maximum value of core flux density as per the B-H curve of the core material used [14]. Consequently, beyond 12% eccentricity, the alteration in the average point flux density is minimal. *Figure 2* shows the 2-D sectional view which shows stator core, stator slot, rotor core, rotor slot and air gap. There

FOREX Publication
Open Access | Rapid and quality publishing
International Journal of Electrical and Electronics Research (IJEER)
Research Article | Volume 13, Issue 2 | Pages 346-352 | e-ISSN: 2347-470X

are two poly lines marked in *figure 2* which has been passed through the stator core and rotor core to find flux density. Similarly *figure 3* shows the poly lines to determine stator teeth and rotor teeth flux density. The poly lines are passing through stator teeth and rotor teeth for this case.

Table 2. Average value of flux density in direction of eccentricity in the air gap

Type of Methods	Flux density at a point in Tesla		
	10%	12%	13%
Static	1.6631	1.733	1.733
Dynamic	1.6613	1.737	1.737
Mixed	1.6620	1.735	1.735

2.3. Core Losses by Experiments

Jyoti Switchgear Pvt. Ltd (JSL) in Mogar, Gujarat, India has produced both healthy and eccentric three-phase squirrel cage induction motors *fig.4*. Practically the static eccentricity on the rotor is made by tapered machining of the rotor. It means that the air-gap at one side is smaller and larger at the other side. While dynamic eccentricity of the air gap is made by machining of the rotor by shifting its centre. This will create an uneven air gap throughout the periphery while rotating. For mixed eccentricity, the tapered machining rotor is interchanged with the dynamic stator core.

These motors underwent No load tests and loss separation tests in accordance with IEEE 112 standard to determine the no load losses for static eccentricity of 12%, dynamic eccentricity of 12%, and mixed eccentricity of 12%. Variable voltage needs to be applied to separate the iron losses, friction and windage losses. A graph of voltage square versus power losses needs to be plotted. The diametric dimensions have been measured using micrometre and voltage, current, input power have been measured by using 0.2 class Yokogawa meter.

Figure 4. Experimental Measurement of Core Loss at JSL

The no-load test readings of squirrel cage induction are presented in *table 3* and loss separation test readings are given in *table 4*.

Table 3. No Load Test Readings

Motor Condition	Voltage (volt)	Current (Amp)	Input Power (watt)	Speed (rpm)
Healthy	415	3.48	251	1499
Static	415	3.93	310	1492
Dynamic	415	4.05	295	1495
Mixed	415	4.32	307	1498

Table 4. Mechanical loss and core loss with variable voltage

Supply Voltage (volts)	Constant loss in (W)			
	Healthy	Static	Dynamic	Mixed
440	234	272	249	256
415	203	229	223	216
400	183	203	202	207
360	146	165	158	164
320	113	127	123	129
280	88	97	95	96
240	65	70	74	73
200	47	51	54	54
160	35	40	46	44
120	27	35	32	37

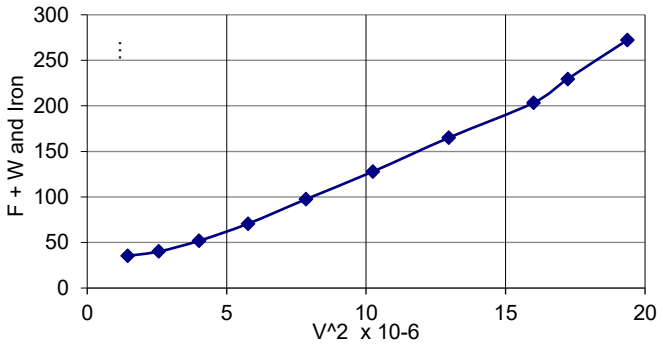

Figure 5. Loss separation curve for 12% static eccentricity

The no-load test determines constant loss for different types of eccentricity by subtracting no-load copper loss from the no load input power reading. The core loss and mechanical Loss can be separated by taking a reading of input power and current by changing the voltage from 125% of rated voltage to the voltage where further reduction in voltage increases the current as shown in *table 5*. Then, plot the constant Loss Vs voltage and extend the graph to the zero voltage. The *figure 5* shows the graph of the loss separation test for the 12% of static eccentricity. The graph is extended to separate the mechanical losses from the constant loss.

FOREX Publication
Open Access | Rapid and quality publishing
International Journal of Electrical and Electronics Research (IJEER)
Research Article | Volume 13, Issue 2 | Pages 346-352 | e-ISSN: 2347-470X

3. RESULTS AND DISCUSSION

In *table 2*, a comparison between the analytical and Ansys results of the loss coefficients is presented. Using the calculated coefficients, the eddy current loss, hysteresis loss, and additional loss are determined using the analytical method and compared with simulation and experimental results. *Figure 6* and *figure 7* depict a comparison between the analytical and simulation results of the stator core and stator teeth flux density at 12% dynamic eccentricity, respectively. The stator core Similarly, *figure 8* and *figure 9* illustrate the analytical and simulation results of the rotor core and rotor teeth flux density at 12% dynamic eccentricity, respectively.

The core and teeth flux density results are obtained by numerical method with the consideration of poly line as shown in *figure 2* and *figure 3*. Analytically core and teeth flux density waves are derived from an analytical result of an average air gap flux density. Once the average air gap flux density has been determined for both healthy and eccentric conditions, obtaining the flux density in the core and teeth follows seamlessly through induction motor design calculations [15].

Figure 6 and *figure 7* depict the stator core and stator teeth flux density. *Figure 8* and *figure 9* depict the rotor core and rotor teeth flux density. The flux density through the core and teeth fluctuates spatially because of various factors including geometry of the core, the arrangement of the windings, and the magnetic properties of the core material. In the case of healthy induction motor, distribution of flux density is relatively uniform but when eccentricity exists, the air gap length between the stator and rotor varies, which changes the magnetic coupling between them. Due to these variations in the air gap length, it results in fluctuations in the magnetic flux flowing through the core and teeth, resulting in a non-uniform flux density distribution. Due to the shorter air gap distance, the flux density tends to be higher close to the areas of maximum eccentricity, resulting in localized flux density peaks. On the other hand, the flux density decreased in locations with low eccentricity, creating valley points.

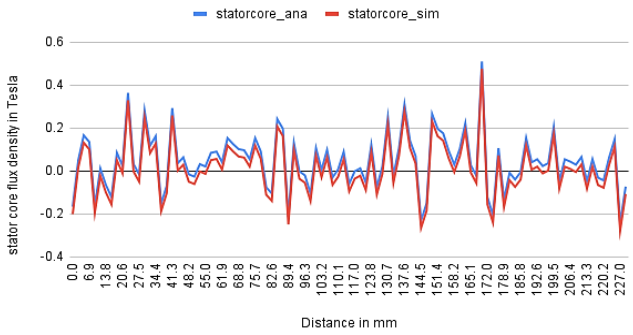

Figure 6. Stator core flux density at 11% static eccentricity

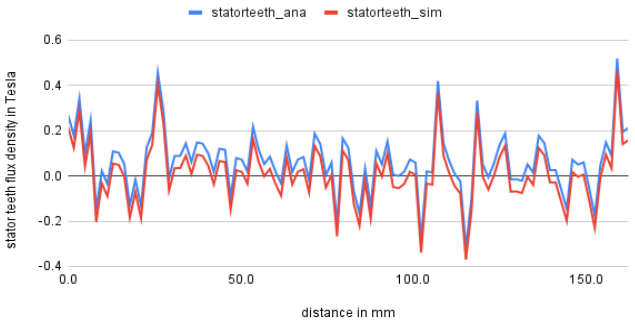

Figure 7. Stator teeth flux density at 12% dynamic eccentricity

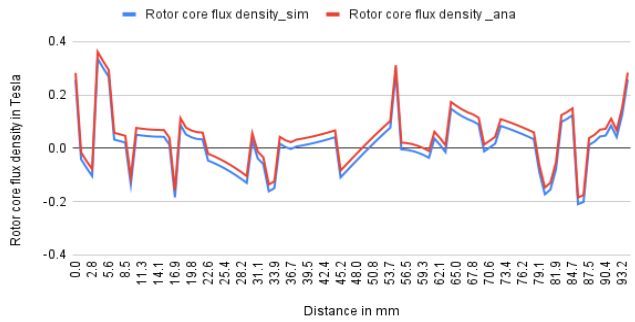

Figure 8. Rotor core flux density at 12% dynamic eccentricity

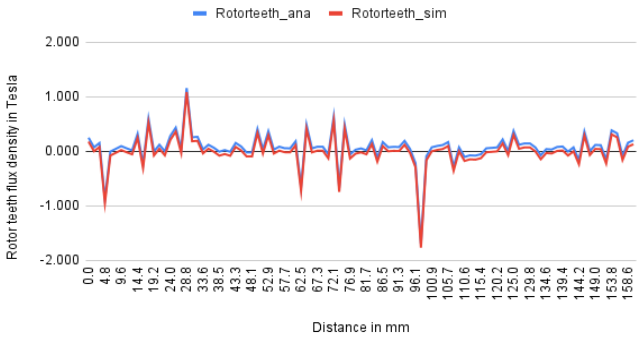

Figure 9. Rotor teeth flux density at 12% dynamic eccentricity

Table 5. Core losses at various degrees of eccentricities in watt

Type of Eccentricity	Core Loss in watt					
	10% Eccentricity		12% Eccentricity		13% Eccentricity	
	Analytical	Simulation	Analytical	Simulation	Analytical	Simulation
Static	192.17	191.87	192.22	192.13	192.87	192.36
Dynamic	191.07	190.86	191.13	191.48	191.69	191.52
Mixed	194.90	192.58	194.92	193.14	194.84	193.38

FOREX Publication
Open Access | Rapid and quality publishing
International Journal of Electrical and Electronics Research (IJEER)
Research Article | Volume 13, Issue 2 | Pages 346-352 | e-ISSN: 2347-470X

According to *table 5*, as the degree of eccentricity increases, so does the core loss. However, at 13% eccentricity, the flux density approaches saturation, indicating that the maximum flux density does not increase with eccentricity, thereby affecting core loss. The analytical and numerical core loss findings were experimentally validated at 12% static, 12% dynamic, and 12% mixed eccentricity levels, as detailed in *table 6* while *table 7* represents a comparison of mechanical losses at same eccentricity levels. Mechanical losses are notably higher in cases of static eccentricity due to the increased radial load on the bearing while dynamic eccentricity varying load and force on bearing. This variation causes fluctuations in mechanical losses.

Table 6. core losses at 12% static, 12% dynamic, and 24% mixed Eccentricity

Type of Methods	Core Loss in watt			
	Healthy	Static	Dynamic	Mixed
Analytical	181.62	192.22	191.08	184.7
Simulation	182.57	192.13	191.48	185.23
Practical	183.37	194.92	193.14	186.9

Table 7. Mechanical losses at 12% of static, 12% of dynamic and 24% of mixed Eccentricity

Type of Methods	Mechanical Loss in Watt			
	Healthy	Static	Dynamic	Mixed
Analytical	24.56	35.67	31.98	36
Practical	22	33.45	30.02	35.87

Table 8. constant losses at 12% static 12% dynamic, and 24% mixed Eccentricity

Type of Methods	Constant Loss in Watt			
	Healthy	Static	Dynamic	Mixed
Analytical	206	227.89	223.06	220.7
Practical	205.37	228.37	223.16	222.77

After analysis of individual components *i.e.* core loss and mechanical loss of constant loss, *table 8* represented variation of constant losses with the types of eccentricity.

4. CONCLUSION

The rotor eccentricity mainly affects the uniform air gap distance between the stator- rotor and ultimately to uniform distribution pattern through the motor. Different types of eccentricity have different effects. Static eccentricity leads to a non-uniform flux density distribution, with a higher flux density at the minimum air gap distance and lower density on the opposite side. The flux density distribution becomes more asymmetrical and a complex compared to other types of eccentricity because it varies the flux density distribution in radial as well as in tangential directions. While in case of dynamic eccentricity, the flux density distribution experienced dynamic variation in the air gap distance. This variation induced by eccentricity, which led to an uneven magnetising force on stator as well as rotor. In short, any type of eccentricity converts uniform magnetic field distribution pattern to non-uniform distribution pattern through the different components of motor. This non uniformity leads a various effect like an uneven magnetising force on the rotor and stator core, mechanical vibration, increased mechanical stress on motor components, and increased temperature rise, increased losses and premature failure of motor components. Due to these reasons, motor efficiency, stability and performance are reduced.

By other way different types of eccentricities generate a specific harmonic signature in the air gap magnetic field and the stator current. The magnitude of these harmonics is affected by the degree of the eccentricity and the load conditions. As the eccentricity level is increases the core loss components also increased.

An eccentricity exerted an additional load on the bearing, due to this no-load current, and the mechanical losses of the motor increased. The increments in stator current loss and mechanical loss increased the overall constant loss of the motor, which directly affected the efficiency of the motor. The computation of constant loss, separation of core loss and mechanical loss with three different types of eccentricity in an induction motor has been computed with three different approaches, successfully. This investigation can extend with load conditions and also included the skin effect in analysis of core loss.

Conflicts of Interest Statement:

Manuscript title: Analysis of Constant Losses of three-phase squirrel cage induction motor with different types of Eccentricity under no load operating condition

The authors whose names are listed in this paper certify that they have NO affiliations with or involvement in any organization or entity with any financial interest (such as honoraria; educational grants; participation in speakers' bureaus; membership, employment, consultancies, stock ownership, or other equity interest; and expert testimony or patent-licensing arrangements), or non-financial interest (such as personal or professional relationships, affiliations, knowledge or beliefs) in the subject matter or materials discussed in this manuscript.

REFERENCES

[1] A. Polat, Y. D. Ertu, and L. T. Ergene, "Static, Dynamic and a Mixed Eccentricity y of Induction Motor," pp. 284–288, 2015.

[2] B. C. F. Smith and M. Eric, "The Losses in Induction Motors Arising from Eccentricity of the Rotor.," vol. 46, 1911.

[3] X. Li, J. Liu, C. Li, J. Hong, and D. Wang, "Research on the influence of air-gap eccentricity on the temperature field of a motorized spindle," Mech. Sci., vol. 12, no. 1, pp. 109–122, 2021.

[4] J. C. Akiror, T. Rahman, and P. Pillay, "Progress on formulas for core loss calculations," Proc. - 2012 20th Int. Conf. Electr. Mach. ICEM 2012, pp. 1803–1809, 2012.

[5] Mendagri, "Improved Design of Motors for Increased Efficiency in Residential and Commercial Buildings," vol. Vol 49, no. Iraqi Journal of Science, pp. 69–73, 2008.

International Journal of
Electrical and Electronics Research (IJEER)
Research Article | Volume 13, Issue 2 | Pages 346-352 | e-ISSN: 2347-470X

[6] B. Tekgun, "Analysis, Measurement and Estimation of the Core Losses in Electrical Machines," p. 137, 2016.

[7] A. Krings, S. Nategh, A. Stening, H. Grop, O. Wallmark, and J. Soulard, "Measurement and modeling of iron losses in electrical machines," 5th Int. Conf. Magn. Metall. WMM'12, no. January, pp. 101--119, 2012.

[8] J. Li, T. Abdallah, and C. R. Sullivan, "Improved calculation of core loss with nonsinusoidal waveforms," Conf. Rec. - IAS Annu. Meet. (IEEE Ind. Appl. Soc., vol. 4, pp. 2203–2210, 2001.

[9] L. T. Mthombeni and P. Pillay, "Core losses in motor laminations exposed to high-frequency or nonsinusoidal excitation," IEEE Trans. Ind. Appl., vol. 40, no. 5, pp. 1325–1332, 2004.

[10] Z. Zhao, X. Hu, Z. Bi, M. Xu, X. Ma, and P. Zhang, "Calculation of core loss under distorted flux density with minor hysteresis loops for laminated steel structure," AIP Adv., vol. 10, no. 7, pp. 1–8, 2020.

[11] D. M. Ionel, M. Popescu, S. J. Dellinger, T. J. E. Miller, R. J. Heideman, and M. I. McGilp, "On the variation with flux and frequency of the core loss coefficients in electrical machines," IEEE Trans. Ind. Appl., vol. 42, no. 3, pp. 658–667, 2006.

[12] N. Alatawneh, T. Rahman, S. Hussain, D. A. Lowther, and R. Chromik, "Accuracy of time domain extension formulae of core losses in non-oriented electrical steel laminations under non-sinusoidal excitation," IET Electr. Power Appl., vol. 11, no. 6, pp. 1131–1139, 2017.

[13] Bpom Ri, "Model for core loss prediction at high frequency and high flux density," Thesis, no. September, pp. 1–94, 2012.

[14] E. Steel, "isovac 600-50 A HC The specialist with high," pp. 1–7, 2018.

[15] A.K. Sawhney, "A Course in Electrical Machine Design," Dhanpat Rai & Co.(P) Ltd., reprint 2013. pp 10.1 - 10.97